scientific reports

Check for updates

OPEN

The factors affecting noontime ionospheric NmF2 equinoctial asymmetry over mid-latitude regions

Andrey V. Mikhailov[1] & Loredana Perrone[2]✉

Mid-latitude semiannual noontime NmF_2 peaks were analyzed at four North Hemisphere (Boulder, Rome, Wakkanai, Juliusruh) and two South Hemisphere (Hobart, Port Stanley) stations. Aeronomic parameters responsible for the observed NmF_2 variations were obtained solving an inverse problem of aeronomy with the original THERION method. The NmF_2 autumnal peak on average is larger than the vernal one in both Hemispheres under solar minimum. The observed NmF_2 difference in the two peaks is attributed to the difference in thermospheric parameters not related to solar and geomagnetic activity. The vernal peak may occur in the course of three months in both Hemispheres while the occurrence of the autumnal peak is confined by two months. The abundance of atomic oxygen [O] plays the leading role in the difference between NmF_2 in the two peaks. A two-hump NmF_2 variation with a trough in December-January (Northern Hemisphere) is a manifestation of low [O] concentration in December/January relative to October/November values rather than the solar zenith angle effect. The empirical (based on observations) MSISE00 model indicates the global increase of the total atomic oxygen abundance during equinoxes which cannot be attributed to any redistribution of [O] in the thermosphere as we have the absolute global scale [O] increase. The downward transfer of [O] by eddy diffusion is the process which can globally control the amount of [O] in the thermosphere. Anyway it is not seen any other way to explain the global increase of the total amount of atomic oxygen during equinoxes.

Variations of mid-latitude noontime monthly median foF_2 in the course of the year manifest a combination of three components: annual - responsible for "December anomaly", seasonal - responsible for "Winter anomaly", and semiannual component responsible for semiannual foF_2 peaks. This was shown in the extensive morphological analysis[1–3]. The December anomaly with global foF_2 values larger in the vicinity of December solstice than around the June one was firstly reported by the authors[4,5]. Although it is obvious that the effect is related to the Sun-Earth distance today after many decades a formation mechanism of December anomaly is still discussed in the literature[6–8]. The explanation of the Seasonal anomaly with winter foF_2 values larger than summer ones in terms of yearly variations of thermospheric composition was proposed[9,10]. Later this idea was confirmed by model simulations[11]. Further attempts in this direction have resulted in a beautiful explanation of seasonal variations in the ionospheric F_2-region[12]. The mechanism includes global from summer to winter Hemisphere thermospheric circulation, the total insolation, and auroral heating with its crucial role in longitudinal/latitudinal foF_2 yearly variations. Available global ionospheric and thermospheric observations in general confirm the validity of this mechanism.

The situation with semiannual variations in thermosphere and ionosphere looks more complicated. The semiannual foF_2 variations in the course of the year were described long ago[1], while semiannual variations in the thermosphere were revealed using harmonic analysis of satellite drag observations[13]. The authors[12] have considered 6 mechanisms of semiannual variations ever proposed. The final conclusion of their analysis – "the circulation-driven mechanism provides a reasonably complete explanation of the observed pattern of F_2 layer annual and semiannual quiet-day variations". However, a comparison of STIP simulation results used in their analysis with monthly median NmF_2 observations manifest a difference up to factor of 2 during equinoxes even at a normal mid-latitude station Slough for noontime[14]. Further, STIP simulations give equal magnitudes for equinoctial NmF_2 peaks while they may be different in observations. Therefore global thermospheric circulation

[1]Pushkov Institute of Terrestrial Magnetism, Ionosphere and Radio Wave Propagation (IZMIRAN), Troitsk 108840, Moscow, Russia. [2]Istituto Nazionale di Geofisica e Vulcanologia (INGV), Rome 00143, Italy. ✉email: loredana.perrone@ingv.it

alone is not sufficient to provide a satisfactory (at the quantitative level) explanation to semiannual NmF_2 variations. Noontime NmF_2 at middle latitudes manifest the state of the surrounding thermosphere (mainly atomic oxygen concentration) therefore observed semiannual foF_2 peaks directly point to the corresponding peaks in atomic oxygen and neutral density which is mainly presented by atomic oxygen at F_2-layer heights. Therefore problems with the description of semiannual foF_2 peaks mean problems with the description of thermospheric parameters during equinoxes.

The most straightforward explanation of semiannual peaks in neutral gas density, atomic oxygen and correspondingly in foF_2 is eddy diffusion with its minimal intensity around equinoxes. The possibility of eddy diffusion to control the thermospheric neutral composition is known long ago[15–17]. Unfortunately up to now very few are known about spatial and temporal variations of this process. The 'thermospheric spoon' mechanism[18] tells about minimal mixing of the thermosphere during equinoctial periods seemingly confirming the idea of decreased eddy diffusion during equinoxes. In his mechanism a semiannual variation of O/N_2 is generated by the inter-hemispheric circulation. TIE-GCM simulations qualitatively reproduce O/N_2 and neutral density semiannual variations but they are much smaller than observed ones[19]. This was also mentioned in relation with a comparison of STIP simulation results with NmF_2 observations[14].

Further steps were done by the authors[19,20] who varying eddy diffusion coefficient have fitted TIE-GCM and TIME-GCM model simulation results to satellite neutral density observations. Both analyses manifested yearly variations of eddy diffusion (K_{edd} coefficient) with minima around equinoxes[20]. Recent results[21] are also inclined to the same conclusion: "Results produced by TIE-GCM are closest to the observations when seasonally varying eddy diffusivity is considered in the model." Of course, technically it is always possible to prescribe the difference between simulation results and observations to any unknown process. But who could vouch for the fact that incorrect K_{edd} specified in the original versions of TIE-GCM and TIME-GCM models is the only drawback that prevents the simulation results to coincide with neutral density observations? Along with this yearly varying eddy diffusion looks as the most plausible basic mechanism to explain global occurrence of semiannual variations in the thermosphere and correspondingly in the F_2-region as this is discussed in the paper.

The aims of the paper may be formulated as follows.

1. To check is there a statistically significant difference between vernal and autumnal foF_2 peaks at middle latitudes during noontime hours.
2. To specify the aeronomic parameters responsible for the difference between vernal and autumnal foF_2 peaks.
3. To discuss possible mechanism(s) forming the vernal and autumnal foF_2 peaks in the thermosphere-ionosphere system.

Observations and results

It is well-known that vernal and autumnal foF_2 peaks manifest large variations depending on geophysical conditions. We confined our analysis by four mid-latitude North Hemisphere stations Boulder (40.0^0N, 254.7^0E, $\Phi = 48.1^0$ Φ is the magnetic latitude) Rome (41.8^0N, 12.5^0E, $\Phi = 41.9^0$), Wakkanai (45.4^0N, 141.7^0E, $\Phi = 36.9^0$), Juliusruh (54.6^0N, 13.4^0E, $\Phi = 54.0^0$) and two mid-latitude South Hemisphere stations Hobart (42.9^0S, 147.3^0E, $\Phi = -50.2^0$) and Port Stanley (51.7^0S, 302.2^0E, $\Phi = -42.0^0$), located in different longitudinal sectors with respect to the magnetic pole. Figure 1 as an example gives noontime monthly median foF_2 yearly variations for similar geophysical conditions under moderate solar and geomagnetic activity but quite different foF_2 variations during equinoctial periods. It is seen that the larger foF_2 peak may occur either in spring or in autumn.

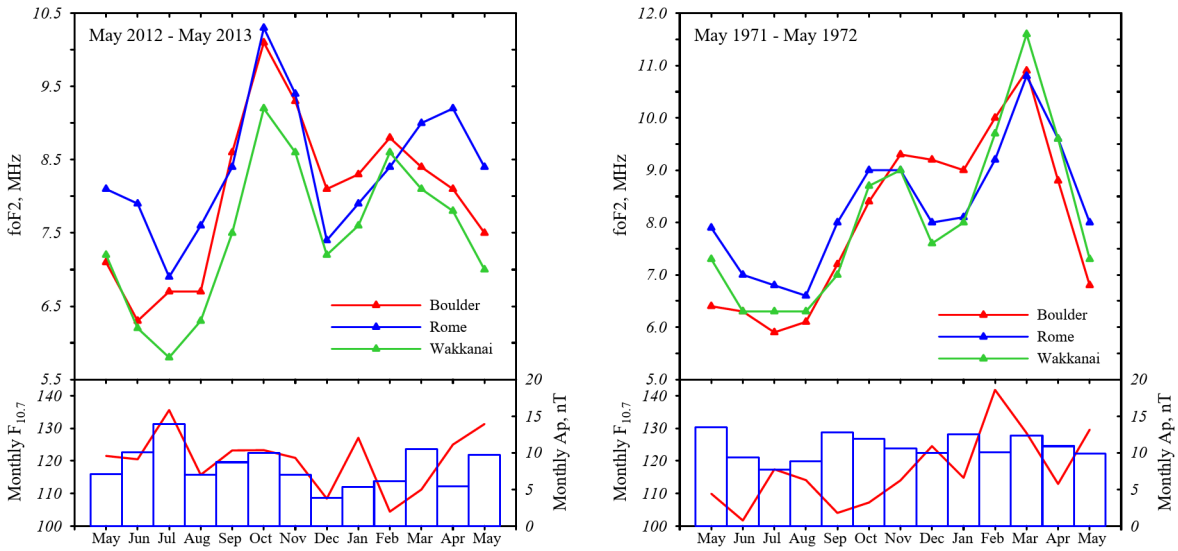

Fig. 1. Observed noontime monthly median foF_2 variations in three longitudinal sectors for two periods with similar monthly $F_{10.7}$ and Ap indices (lower panels) but different foF_2 equinoctial peaks.

It is known that semiannual foF_2 variations dominate at lower latitudes and in the Southern Hemisphere while the contribution of seasonal component increases with geomagnetic latitude and semiannual foF_2 peaks may merge to create a single winter foF_2 maximum[12,14,22,23].

For this reason the vernal foF_2 peak may be often absent at Boulder, a 'near-pole' station. Therefore, we have selected only years when the vernal peak is clearly present in yearly foF_2 variations. For this reason the number of points at Boulder is less compared to Rome for the same (1958–2022) period in question. Figure 2 gives years with monthly median foF_2 used at each station in our analysis.

Electron concentration in the noontime mid-latitude F_2-layer maximum $NmF_2 \sim I_{EUV} \times [O]^{4/3}$ where $NmF_2 = 1.24 \times 10^4 (foF_2)^2$, I_{EUV} is the intensity of ionizing EUV radiation, atomic oxygen concentration [O] is taken at a fixed height in the thermosphere[24]. According to theory, solar I_{EUV} and atomic oxygen are the main contributors to daytime mid-latitude NmF_2.

The vernal and autumnal foF_2 peaks are separated by half of a year in time and solar ionizing EUV radiation is different in two peaks especially during rising and falling phases of a solar cycle. Therefore at first, it is necessary to remove the dependence on solar EUV impact. Calibrated total solar EUV (100–1200) Å flux observations are available for the (2002–2017) period[25]. Observed monthly median EUV manifests a good correlation with the effective $F_{10.7eff} = (F_{10.7\ mon} + F_{10.7\ 3mon})/2$ solar index. A similar solar activity index is used in the EUVAC model[26]. In our case the correlation coefficients between monthly median EUV and $F_{10.7eff}$ is $\sim 0.986 \pm 0.02$ for the equinoctial months. According to the Ceddok scale this is practically a functional dependence and ~ 97% of the EUV variability is explained by $F_{10.7eff}$. Therefore monthly $F_{10.7eff}$ may be used as a proxy for monthly solar EUV radiation for the periods not covered with EUV observations[25]. The reduced NmF_2/EUV values may be further reduced bearing in mind that the amount of produced atomic oxygen via O_2 dissociation depends on the intensity of FUV solar radiation as $[O] \sim I_{diss} \times [O_2]$. The Schumann-Runge continuum is actually the major cause of the O_2 dissociation above 100 km. The characteristic time of this process $\tau_{dis} \approx 1/J_{O2} < 3$ days above 120 km height[27], i.e. this is a fairly fast process and month-to-month variations of the atomic oxygen abundance should depend on month-to-month variations of the intensity of dissociation radiation. A recently developed model of solar EUV and FUV radiation[28] is based on HLα (λ = 1216 Å) solar emission as the input parameter. The model shows that the intensity of FUV radiation is linearly related to HLα. Therefore it is possible to use directly observed HLα[29], also LISIRD database https://lasp.colorado.edu/lisird/data/composite_lyman_alpha/) as an indicator of dissociation radiation for the NmF_2/EUV ratio further reduction. The results with double reduced monthly median NmF_2 values are given in Fig. 3.

Vernal foF peaks may occur in the course of three months while autumnal peaks occur only during two months (see later). For this reason the maximal reduced NmF_2/EUV/HLα value over February-April was considered as the vernal peak, while the maximal NmF_2/EUV/HLα value over October-November was considered as the autumnal peak in the Northern Hemisphere. Seasons are shifted by 6 months in the Southern Hemisphere. Hobart manifests very unusual foF_2 yearly variations with the main and well-pronounced autumnal peak always in April and a secondary smaller vernal peak which may or may not occur in the course of 5 months from August to December. However, we analyzed only peaks that occurred in the vicinity of the vernal equinox in August-October. All cases are divided into three levels of solar activity: maximal ($F_{eff} > 150$), medium ($110 \le F_{eff} \le 150$), and minimal ($F_{eff} < 110$). The EUV flux is used in 10^{10} ph $cm^{-2}s^{-1}$ and HLα flux in 10^{11} ph $cm^{-2}s^{-1}$ units.

Points in Fig. 3 are distributed with respect to the bisector which manifests the absence of a difference between vernal and autumnal NmF_2/EUV/HLα peak values. Figure 3 gives that points are clustering around the bisector under elevated and high solar activity while the points are mainly located above the bisector under low solar activity. This means that the autumnal NmF_2/EUV/HLα peak is on average larger than the vernal peak under solar minimum. All points are above the bisector at Hobart for any level of solar activity.

Apart from the dependence on solar radiation, monthly median NmF_2 also depends on geomagnetic activity via neutral composition, mainly atomic oxygen. The relationship of NmF_2 with monthly Ap indices is

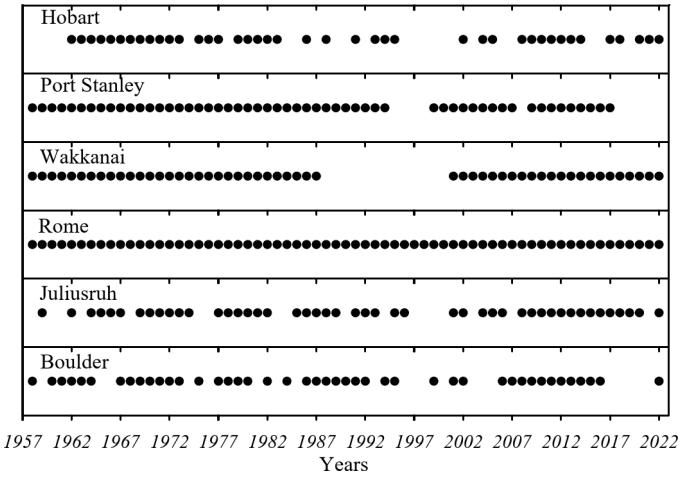

Fig. 2. Years with monthly median foF_2 at each station used in our analysis.

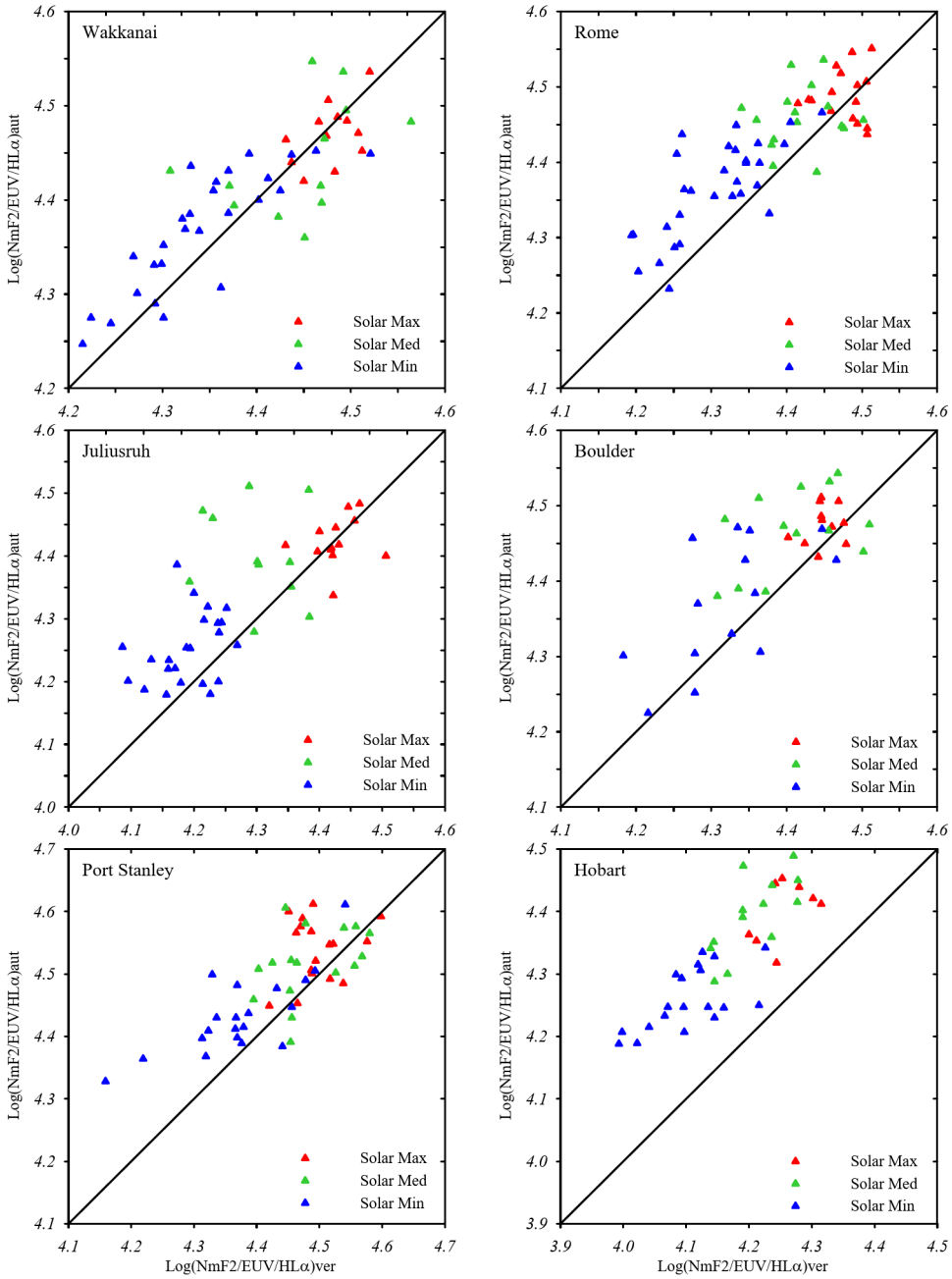

Fig. 3. Scatter plots of reduced monthly median NmF_2/EUV/HLα autumnal values versus vernal ones at six stations for three levels of solar activity.

not straightforward but depends on solar activity, season, local and storm time, and geomagnetic latitude of a station. Moreover, unlike NmF_2 day-to-day variability when geomagnetic activity impact is well-pronounced, geomagnetic effects may not be seen in monthly median NmF_2 due to the very procedure of NmF_2 medians derivation. Monthly median NmF_2 clearly manifests the disturbance effects if only half of days in a month were really disturbed and this is not often. For this reason NmF_2 monthly median empirical models like IRI[30] or the model[31] do not include the dependence on geomagnetic activity.

However the impact of geomagnetic activity on monthly median NmF_2 under different levels of solar activity may be interesting in the framework of our analysis. Although this impact is small due to a weak relationship between noontime monthly median NmF_2 and Ap indices Table 1 gives the results of such correlation analysis.

Table 1 gives that correlation coefficients between NmF_2/EUV/HLα and monthly Ap in general are low although they may be significant. Positive correlation coefficients take place under solar minimum while they are negative (when significant) under solar maximum. In general the correlation is ranging between moderate and weak on the Ceddok scale. For this reason any further reduction of NmF_2/EUV/HLα on geomagnetic activity gives no visible results even under solar minimum – the number of points above the bisector in Fig. 3 is not

Station	Solar Minimum			Solar Maximum		
	Corr. coeff.	Significance	Correlation	Corr. coeff.	Significance	Correlation
Boulder	+0.631 ± 0.237	99.9%	Notice/Moder	-0.217 ± 0.421	Insign.	Absent
Rome	+0.494 ± 0.188	99.9%	Moderate	-0.009 ± 0.302	Insign.	Absent
Juliusruh	+0.263 ± 0.278	Insign.	Absent	-0.336 ± 0.307	95%	Weak/Absent
Wakkanai	+0.494 ± 0.212	99.9%	Moder/Weak	-0.364 ± 0.316	96%	Moder/Absent
P. Stanley	+0.474 ± 0.234	99.9%	Moder/Weak	+0.053 ± 0.303	Insign.	Absent
Hobart	+0.201 ± 0.297	Insign.	Absent	+0.029 ± 0.109	Insign.	Absent

Table 1. Correlation coefficients between NmF_2/EUV/HLα and monthly Ap indices under solar minimum and maximum. The total correlation is estimated on the Ceddok scale.

Stations	Vernal peak			Autumnal peak	
	February	March	April	October	November
Wakkanai (52)	19 (37%)	33 (63%)	0	35 (67%)	17 (33%)
Rome (65)	27 (41%)	31 (48%)	7 (11%)	56 (86%)	9 (14%)
Juliusruh (47)	36(77%)	9(19%)	2(4%)	20(43%)	27(57%)
Boulder (39)	23 (59%)	16 (41%)	0	10 (26%)	29 (74%)
	August	**September**	**October**	**March**	**April**
Port Stanley(55)	0	3(5%)	52(95%)	14(25%)	41(75%)
Hobart (41)	8(20%)	23(56%)	10(24%)	0	41(100%)

Table 2. The probability (in %) of NmF_2/EUV/HLα peaks occurrence during vernal and autumnal months. The total number of analyzed years at a given station is given in brackets.

increased. Therefore the distribution of points given in Fig. 3 may be considered as the final one for our further analysis.

Figure 3 indicates a systematic dependence of autumnal NmF_2/EUV/HLα versus vernal ones. All correlation coefficients are significant at the 99.9% confidence level and vary from 0.680 ± 0.168 at Boulder to 0.896 ± 0.060 at Hobart with the correlation ranging between noticeable and close according to the Ceddok scale.

Another interesting aspect is the timing of vernal and autumnal peaks occurrence. Table 2 gives the number of peak occurrences at six stations for vernal and autumnal months over all years in question. Double reduced NmF_2 were used in this statistics.

Table 2 manifests that the vernal peak may occur in the course of three months in both Hemispheres while the occurrence of the autumnal peak is confined by two months. Hobart station demonstrates an interesting behavior. Along with results given in Fig. 3 where all autumnal points are larger than vernal ones under all solar activity levels, Table 2 shows that all these autumnal points belong to one month, April.

Summarizing the morphological part of our analysis it is possible to conclude that the NmF_2 autumnal peak on average is larger than the vernal one in both Hemispheres at least under solar minimum. The autumnal NmF_2 peak independently on solar activity always occurs within two months while the vernal peak may occur in the course of three months. An additional analysis has shown that Hobart manifests the main and well-pronounced autumnal peak always in April and a secondary smaller vernal peak which may or may not occur in the course of five months from August to December. This peculiarity of Hobart requires a special analysis.

Interpretation

According to theory day-time mid-latitude NmF_2 manifests the intensity of solar EUV radiation, the state of surrounding neutral composition, and vertical plasma drift related to thermospheric winds[24,32]. The (2008–2009) period was selected for our analysis. That was a deep solar minimum with very low geomagnetic activity. Moreover CHAMP/STAR neutral gas density (ftp://anonymous@isdcftp.gfz-potsdam.de/champ/) and solar EUV observations[25] are available for this period.

Figure 4 gives observed yearly variations of noontime foF_2 at Juliusruh and Port Stanley during July - December 2008 and January - June 2009. Both stations are located in the 'far-from-pole' longitudinal sector. The polynomial approximation of foF_2 variations manifests the results earlier given in Fig. 3 for solar minimum conditions - the foF_2 autumnal peak is larger than the vernal one in both Hemispheres. This difference is not related to solar EUV fluxes which are close for the two periods. Averaged over February-March and October-November daily Ap = 4.93 ± 3.66 nT and 5.38 ± 5.85 nT, correspondingly. Student's t-parameter = 0.499 under the degree of freedom m = 118 indicates the absence of any statistically significant difference between two arrays of Ap indices. Therefore the observed foF_2 difference in the two peaks should be attributed to the difference in thermospheric parameters not related to solar and geomagnetic activity.

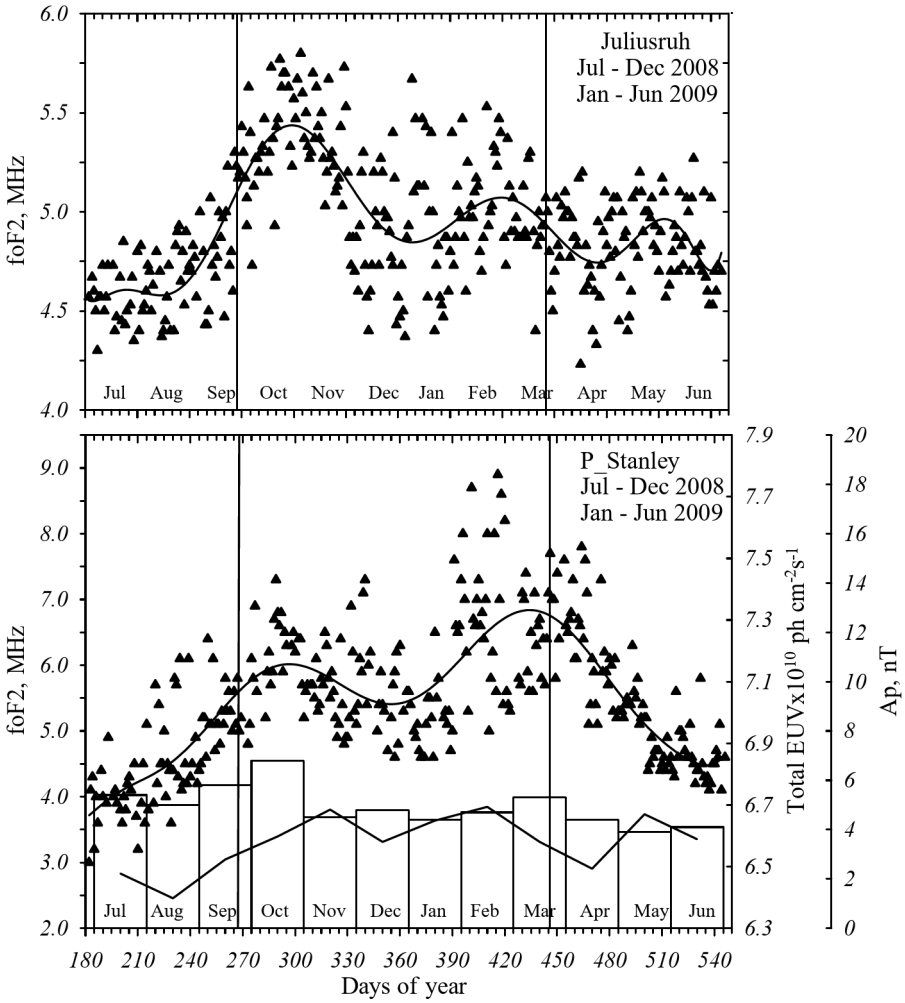

Fig. 4. Yearly variations of noontime foF_2 at Juliusruh and Port Stanley during. July-December 2008 and January-June 2009. Polynomial approximation of observed foF_2 is given for better visualization of yearly variations. Monthly median Ap and total solar EUV variations are given in the bottom of the plot. Vertical lines indicate the dates of equinoxes.

Figure 4 gives that two foF_2 peaks in both Hemispheres are shifted towards the December solstice with respect to the equinoctial dates. This clearly indicates the contribution of the annual component responsible for the December anomaly in atomic oxygen and foF_2 yearly.

variations[8]. However this does not explain the excess of the autumnal foF_2 peak over the vernal one. At Port Stanley the autumnal peak occurs in March i.e. two months later than the peak of the annual component occurring in December.

Aeronomic parameters responsible for the formation of daytime mid-latitude F_2-layer are required to explain the observed yearly NmF_2 variations. Our method THERION[33] with further improvements[34] was used to specify these parameters. The method was repeatedly used in our previous publications [34,35,36] and its description is not given here. The idea is based on solving an inverse problem of aeronomy to extract a self-consistent set of aeronomic parameters from bottom-side Ne(h) profile and satellite neutral gas density observations. Among these parameters are [O] and $[N_2]$ column densities calculated above the height with column $[N_2]$ of 10^{17} cm^{-2} [37] and basic aeronomic parameters in the F_2-layer maximum which are obtained in the course of the fitting process. The results of calculations for Juliusruh are given in Fig. 5. Figure 5 gives that the main peak in the atomic oxygen column abundance takes place in November and the other not a peak but an inflection point is in February. In accordance with present-day understanding (see Introduction) the November peak is a sum of three components: semi-annual, seasonal, and annual, while the February inflection point is formed by semi-annual and seasonal components of yearly variations. Yearly NmF_2 variations manifest peaks which are close in time to peaks in column [O] density (Fig. 5b) but they do not exactly coincide. This is understandable as NmF_2 depends on atomic oxygen concentration at the F_2-layer maximum height rather than on column [O] density[38]. The NmF_2 peaks are closer in time to $q(O^+)_{max}$ peaks (Fig. 5b) in accordance with a well-known expression[39]

$$N_m F_2 = 0.75 \frac{q_m}{\beta_m}$$

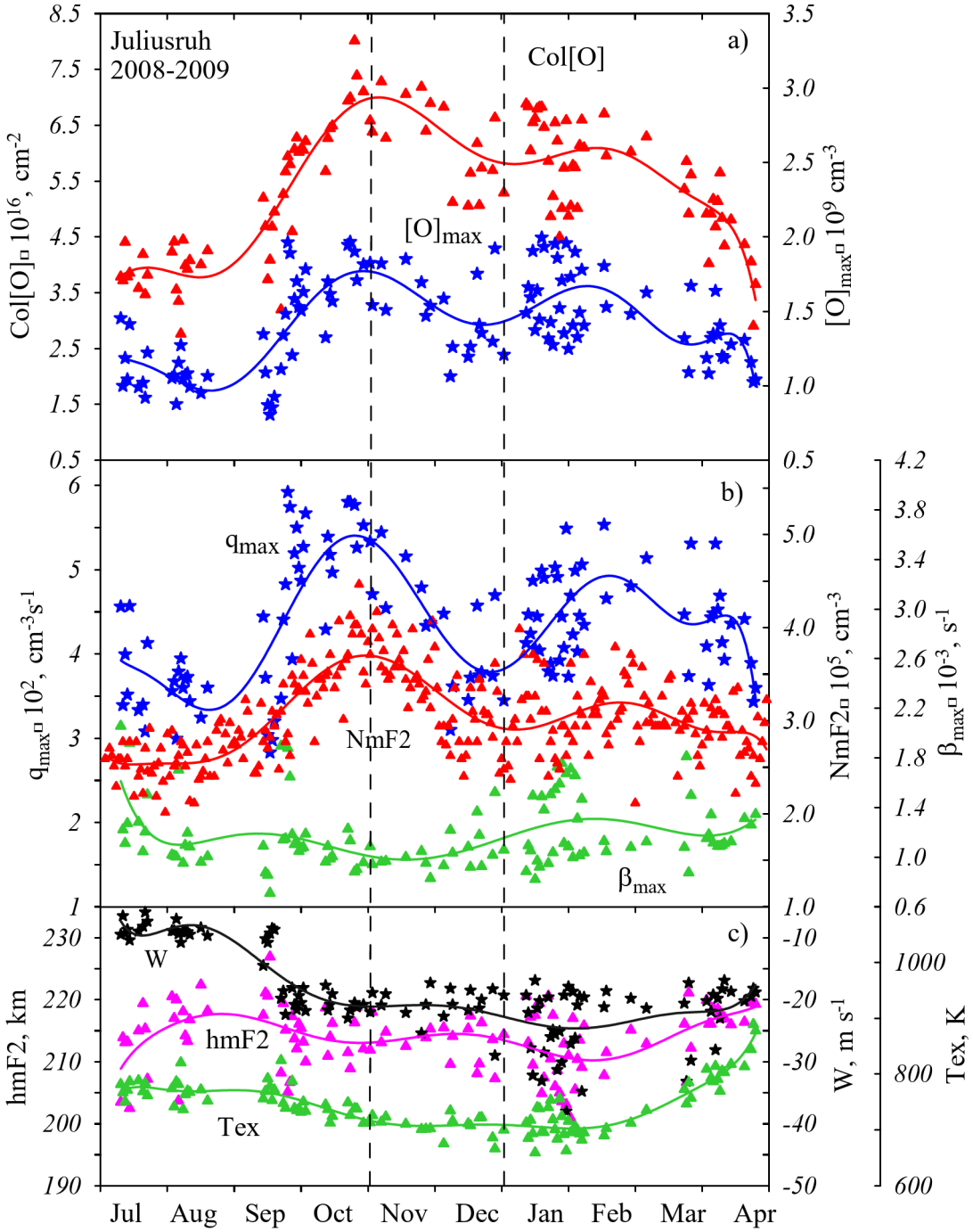

Fig. 5. Noontime aeronomic parameters for the (2008–2009) period. Column atomic oxygen abundance and [O] concentration in the F_2-layer maximum - a); observed NmF_2, total rate of $[O^+]$ ion production q_{max} and linear loss coefficient β_{max} in the F_2-layer maximum – b); vertical plasma drift W, hmF_2, and exospheric temperature Tex – c). Solid lines are polynomial approximations given for better visualization. Vertical dashed lines – 27 October 2008 and 26 December 2008 (see text).

where q_m – O^+ ion production rate and β_m – linear loss coefficient, both taken at h_mF_2. A similar expression can be also obtained using an analytical solution of the stationary continuity equation for electron concentration in the mid-latitude daytime F_2-region[24]. This expression does not take into account the effects of vertical plasma drift W. However it can be used for qualitative estimates. Figure 5,b shows that $q(O^+)_{max}$ is larger in the autumnal NmF_2 peak (October-November) than in the vernal one although $[O]_{max}$ are similar in the two peaks (Fig. 5,a). Partly this is due to different solar zenith angles -63.7^0 in the middle of October and 67.1^0 in the middle of February. An additional contribution to this difference in NmF_2 provides β_{max} which is larger in January-February than in October-November. The difference in β_{max} may be related to different hmF_2 which

Date	$N_mF_2 \times 10^5$, cm^{-3}	$[O]_{col} \times 10^{16}$, cm^{-2}	$q_m \times 10^2$, $cm^{-3}\ s^{-1}$	$\beta_m \times 10^{-3}$, s^{-1}	h_mF_2, km	W, m s^{-1}	EUV, ph $cm^{-2}\ s^{-1}$	χ, deg	Ap, nT
October 10, 2008	3.75	6.49	4.97	1.01	216	-19.1	3.16	62	2
March 17, 2009	3.16	5.36	4.47	1.08	216	-20.6	3.11	56	4

Table 3. Observed and retrieved aeronomic parameters for the two dates in the autumnal and vernal peaks at Juliusruh to demonstrate the leading role of atomic oxygen in the difference between two NmF_2 peaks. The parameters are explained in the text.

Date	$N_mF_2 \times 10^5$, cm^{-3}	$[O]_{col} \times 10^{16}$, cm^{-2}	$q_m \times 10^2$, $cm^{-3}\ s^{-1}$	$\beta_m \times 10^{-4}$, s^{-1}	h_mF_2, km	W, m s^{-1}	EUV, ph $cm^{-2}\ s^{-1}$	χ, deg	Ap, nT
March 18, 2009	5.24	8.37	5.77	7.10	222	-17.9	3.11	50.9	2
October 25, 2008	4.46	6.70	5.43	8.53	222	-17.5	3.10	39.0	1

Table 4. Same as Table 3 but for Port Stanley for the dates in the autumnal and vernal peaks.

are larger in October-November than in January-February (Fig. 5,c). The main contributors to hmF_2 are Tex and vertical plasma drift, W[24,40]. Figure 5,c gives that Tex are practically the same (~ 700 K) for the two periods but W related to horizontal thermospheric winds are different. Downward plasma drifts W are ~ -20 m/s in October-November but W are ~ -25 m/s and even down to -35 m/s in January-February (Fig. 5,c). Stronger downward W transfers O^+ ions to lower altitudes with larger $[N_2]$ and $[O_2]$ concentrations and correspondingly larger $\beta = \gamma_1[N_2] + \gamma_2[O_2]$. Therefore larger $q(O^+)_{max}$ and smaller β_m (which is related to larger hmF_2 via a weaker downward plasma drift W = VnxsinIcosI) in October-November compared to January-February values may be considered as the reasons for larger autumnal NmF_2 peak compared to the vernal one.

The leading role of the atomic oxygen abundance in the NmF_2 difference in two peaks manifests a comparison of 10 October 2008 to 17 March 2009 at Juliusruh. Observed noontime NmF_2 for these dates are close to October/November and February/March noon monthly median NmF_2, correspondingly (Fig.,5b). Observed EUV[25], daily Ap, calculated hmF_2 and W are close for the two dates to exclude as much as possible their possible impact (Table 3).

The NmF_2 difference between two peaks is 18.7% which is mainly the 11.2% difference in q_m and −6% in β_m. It should be noted that the solar zenith angle χ is larger in October than in March however q_m is larger in October indicating the leading role of [O] in the q_m difference between two dates. The autumnal (10 October, 2008) date also manifests larger column atomic oxygen abundance.

Similar results manifests Table 4 for two dates 18 March, 2009 and 25 October 2008 located in the autumnal and vernal peaks at Port Stanley, correspondingly. The observed NmF_2 are close to noon monthly median NmF_2 (Fig. 4). The list of aeronomic parameters is the same as in Table 3.

The NmF_2 difference between two peaks is 17.5% which is mainly the result from larger q_m and smaller β_m on 18 March, 2009 compared to 25 October, 2008. The other parameters (hmF_2, W, and EUV, Ap) are close for the two dates and this should exclude their possible impact on the difference in NmF_2. Similarly Juliusruh the solar zenith angle χ is larger in autumn (18 March) than in spring, however q_m is larger in March indicating the leading role of [O] in the q_m difference between two dates. The autumnal date (March 18) also manifests larger column atomic oxygen abundance compared to the vernal date. Therefore both Hemispheres manifest the dominance of NmF_2 in the autumnal peak over the vernal one and this is due to larger q_m and smaller β_m in autumn.

A two-hump NmF_2 variation with a trough in December-January (Northern Hemisphere) is a key point of yearly NmF_2 variations. Without such a trough we would have a well-pronounced "winter anomaly" with midwinter NmF_2 values larger than summer ones. This type of yearly NmF_2 variation is observed under solar maximum at middle-high latitudes in the Northern Hemisphere and this issue was repeatedly discussed in the literature[14,41].

According to[12] the winter NmF_2 trough is due to large solar zenith angle during midwinter: "The zenith angle effect is especially important in longitudes far from the magnetic poles. Here, the downwelling occurs at high geographic latitudes, where the zenith angle effect becomes overwhelming and causes a midwinter depression of electron density, despite the enhanced atomic/molecular ratio. This leads to a semiannual variation of NmF_2".

However, our analysis shows that solar zenith angle is important but not the only factor leading to the midwinter NmF_2 depression. Table 5 contains necessary aeronomic parameters taken from Fig. 5 to do such estimates. We took 27 October 2008 when $q(O^+)_{max}$ and NmF_2 reached maximal values and 26 December 2008 when both parameters were much smaller. Table 5 gives that the observed NmF_2 depression is ~35% which is mainly resulted from a decrease of $q(O^+)_{max}$ and an increase of β_{max}. Firstly let us check the contribution of the solar zenith angle, χ. To sufficient accuracy for present purposes, the production $q(O^+)_{max}$ may be written as.

$q(O^+)_{max} = I_\infty Ch(Z_{max},\chi)[O]_{max}$.

Date	$NmF_2 \times 10^5$ cm^{-3}	hmF_2 km	$I_\infty \times 10^{10}$ ph cm^{-2} s^{-1}	Zenith angle, deg	$q(O^+)_{max} \times 10^2$ $cm^{-3}s^{-1}$	$[O]_{max} \times 10^9$ cm^{-3}	W m/s	$\beta_{max} \times 10^{-3}$ s^{-1}
27/10/2008	3.82	212	6.62	68.0	5.33	1.82	-22	1.08
26/12/2008	2.83	214	6.70	78.0	3.45	1.21	-19	1.06

Table 5. The list of aeronomic parameters necessary to estimate the contribution of solar zenith angle to the $q(O^+)_{max}$ decrease.

where I_∞ is the total ionization flux at the top of the atmosphere, $[O]_{max}$ denotes the concentration of atomic oxygen at the F_2-layer maximum height, and $Ch(Z_{max}, \chi)$ is the 'Chapman function' of the solar zenith angle at the hmF_2 height.

The production rate $q(O^+)_{max}$ should be reduced on I_∞ and $[O]_{max}$ to estimate the contribution of solar zenith angle to the $q(O^+)_{max}$ decrease. After this reduction the contribution of $Ch(Z_{max},\chi)$ to the $q(O^+)_{max}$ decrease is ~ 4% while the $q(O^+)_{max}$ difference is ~ 54% between the two dates.

Bearing in mind that I_∞ are close for the two dates the $q(O^+)_{max}$ difference is due to the $[O]_{max}$ difference (Table 5). Therefore the observed midwinter NmF_2 through ~ 35% at Juliusruh (Fig. 4,b) is mainly related to the $[O]_{max}$ decrease from 27 October to 26 December. The contributions of β_{max} and W are small compared to $[O]_{max}$ (Table 5). The difference in $[O]_{max}$ cannot be related with different hmF_2 which are close for the two dates (Table 5). Therefore the midwinter NmF_2 trough is a manifestation of low [O] concentration in December-January relative to October/November (Northern Hemisphere) values rather than the solar zenith angle effect.

Table 2 shows that the vernal peak may occur in the course of three months in both Hemispheres while the occurrence of the autumnal peak is confined by two months. This is due to the difference between summer-to-winter and winter-to-summer transitions in the thermosphere. We do not have direct observations of the seasonal transition in global thermospheric circulation but atomic oxygen which is directly related to this circulation may serve as an indicator of this process. According to[42] there are winter and summer types of foF_2 diurnal variations and analyzing day-by-day foF_2 diurnal variations it is possible to specify the dates of summer-to-winter and winter-to-summer transitions in the thermosphere. It was shown[42] that the summer-to-winter foF_2 transition at Juliusruh in 2008–2009 took place within ~ 12 days while the winter-to-summer transition lasted for ~ 36 days i.e. the autumnal transition is much shorter than the vernal one.

Figure 5,(c) gives that the W transition from summer ~ -10 m/s to winter ~ -20 m/s values occurs very fast during one month (September) and this period corresponds to a steep increase in the atomic oxygen abundance (Fig. 5,a) indicating the process of the atomic oxygen transfer from summer to winter Hemisphere. Although W manifests diurnal variation of thermospheric winds which are not responsible for seasonal inter-hemispheric transfer of atomic oxygen[12] nevertheless W indicates seasonal changes in global thermospheric circulation resulting in variation of the atomic oxygen abundance. Vertical drift W does not manifest any pronounced variations during January-April (Fig. 5c) being around ~ -20 m/s. During this period NmF_2 demonstrates small month-to-month and large day-to-day variations (Fig. 5,b). Under such a scatter the NmF_2 peak may occur in any month (February-April) in the vicinity of the vernal equinox.

All analyzed stations (apart from Hobart) manifest the dominance of the autumnal peak over the vernal one only under solar minimum conditions (Fig. 3). This may be related to the geomagnetic activity impact. Low solar activity is normally associated with low geomagnetic activity and low heating of the auroral zone. Therefore global thermospheric circulation is mainly solar driven and along with yearly varying eddy diffusion (see our discussion later) provide the corresponding variations of atomic oxygen when the autumnal [O] is larger than the vernal one. Under elevated and maximal solar activity geomagnetic activity increases resulting in increased auroral heating. A comparison of monthly Ap indices for the (1958–2022) period for the dates with elevated and high solar activity to dates with low activity gives average $Ap = 15.74 \pm 6.68$ nT and $Ap = 11.38 \pm 5.03$ nT, correspondingly, which differ significantly at the 99.9% confidence level according to t - test. There is a linear relationship between Joule heating and Kp indices[43]. In accordance with the well-known F_2-layer storm mechanism [44-49][44–49,12] the $[O]/[N_2]$ ratio (which is directly related to NmF_2) decreases with increasing geomagnetic activity. Therefore depending on the station and the intensity of auroral heating the NmF_2 points may turn out to be above or below the bisector line in Fig. 3 under elevated and high solar activity.

Comparing foF_2 (Fig. 4) and column [O] yearly variations (Fig. 5) it is seen that two peaks are shifted towards the December solstice with respect to the equinoctial dates. This may be related with contribution of the annual component responsible for the December anomaly in atomic oxygen and correspondingly in foF_2 yearly variations. However according to GUVI O/N_2 ratio observations[50] "…in the northern hemisphere (NH) low latitudes, the first "equinox peak" clearly shifts toward the December solstice, whereas in the southern hemisphere (SH) low latitudes, the "equinox peaks" shift toward the June solstice (JS), forming the hemispheric asymmetry characteristics of the annual and semiannual variation". No explanation to such inter-hemispheric asymmetry is suggested by the authors.

Discussion

The undertaken analysis has shown that the difference between vernal and autumnal NmF_2 peaks is mainly due to the difference in the atomic oxygen abundance. Atomic oxygen is totally produced and lost in the upper atmosphere above 70 km[27]. Therefore we will consider variations of the column [O] abundance above this level using the empirical thermospheric model MSISE00[51]. The column [O] abundance, unlike the concentration at

a fixed height does not depend on the neutral temperature height profile therefore this characteristic is more convenient for our analysis.

Let us consider yearly variations of the atomic oxygen abundance given by the empirical (based on observations) thermospheric model MSISE00. It should be noted that the choice of MSISE00 for our analysis rather than MSIS 2.0[52] is not principal. The difference between two models in the thermosphere is not large: " In the thermosphere, N_2 and O densities are lower in NRLMSIS 2.0; otherwise, the NRLMSISE-00 thermosphere is largely retained". With respect to atomic oxygen that is mostly interesting for our analysis, it is said "The upper thermospheric MSIS 2.0 O densities are ~ 10% less overall than MSISE-00". A comparison of MSISE00 and MSIS 2.0 with CHAMP and GOCE neutral density observations has shown that "Overall, MSIS 2.0 mass densities are ~ 2% larger than GOCE and ~ 9% larger than CHAMP". But this difference is within the inaccuracy (10–15)% of CHAMP neutral density observations [53]. A comparison of neutral density yearly variations given by two models just indicates a small systematic bias[52]. On the other hand, GOLD observations of daytime thermospheric effective temperature and $\Sigma O/N_2$ under deep solar minimum from 13 October 2019 to 12 October 2020[54] have revealed obvious differences between observations and MSIS 2.0. Therefore there is no reason to give preference to any of the models.

Figure 6 gives noontime MSISE00 model variations of the total atomic oxygen abundance above 70 km in the European and American longitudinal sectors for both Hemispheres (top panel), and separately for the Northern and Southern Hemispheres under solar maximum (1980) and solar minimum (2009). The years were selected to have close monthly $F_{10.7}$ and Ap indices for both equinoctial periods. The global atomic oxygen abundance mainly manifests semiannual variations with close magnitudes in the two peaks in both sectors under solar maximum and minimum. This is an important result clearly indicating the global increase of the total atomic oxygen abundance during equinoxes. Such an increase cannot be attributed to any redistribution of atomic oxygen in the thermosphere as we have the absolute global scale [O] increase. Another interesting result – the magnitudes of the two peaks are practically equal. This tells us that the dominance of the autumnal peak over the vernal one revealed in our analysis also seen in [O] total abundance in the two hemispheres (Fig. 6, middle and bottom panels) is related to seasonal thermospheric circulation. The annual component which maximizes in the vicinity of the December solstice provides January [O] abundance larger than July one (Fig. 6, top panels). On the other hand, the seasonal component related to the summer-to-winter transfer of [O] is not seen under the global consideration of the atomic oxygen abundance.

Yearly variations of the [O] abundance with the main peak in November and the secondary peak in March are seen in the Northern Hemisphere (see also Fig. 5,a). The Southern Hemisphere manifests semiannual variations

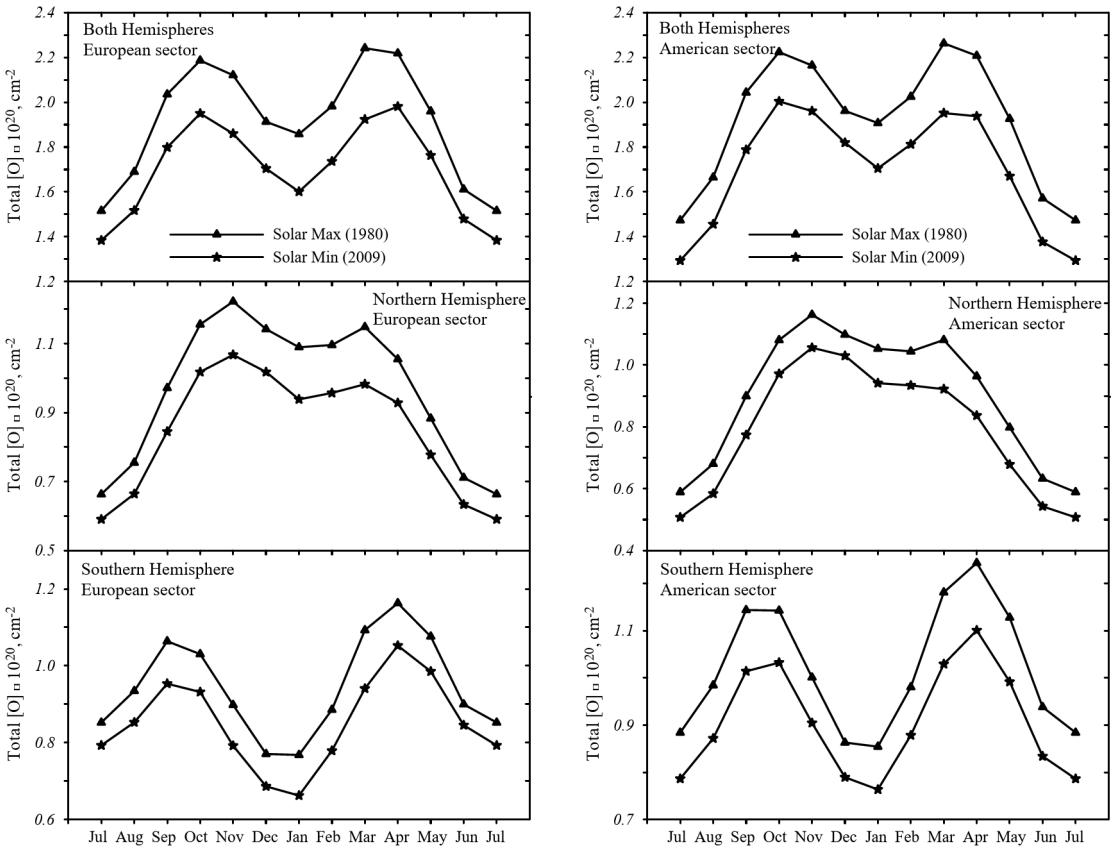

Fig. 6. MSISE00 model variations of the noontime column atomic oxygen abundance above 70 km along the zero meridian in both Hemispheres (top panel) and separately in the Northern and Southern Hemispheres for solar maximum and solar minimum.

with the main peak in April and the secondary in September. Therefore the empirical model MSISE00 confirms our earlier obtained result that the autumnal peak in NmF_2 and column [O] is larger than the vernal one. In accordance with the foF_2 global morphology[14,41,47] the MSISE00 model properly describes seasonal variations of the atomic oxygen total abundance (Fig. 6, middle and bottom panels). Seasonal (winter/summer) difference is large in the Northern Hemisphere where the Seasonal and December components are working in phase and this difference is small in the Southern Hemisphere where two components are anti-phase.

It should be stressed that Fig. 6 (top panel, similar variations may be obtained for other longitudes) gives the global total content of atomic oxygen which cannot be attributed to any seasonal redistribution of [O] by global circulation. Therefore we should speak about the absolute global increase or decrease of the [O] abundance in the course of the year which cannot be attributed to any redistribution of [O] by global circulation as this was suggested[12,18].

An obvious question arises – where does this additional [O] come from around two equinoxes? Atomic oxygen is totally produced and lost in the upper atmosphere above ~ 70 km[27]. Therefore, either this is newly produced [O] or its loss is decreased near equinoxes, there is no other possibility. The rate of [O] production is limited by the intensity of solar far UV radiation which depends only on solar activity[28] and it may be considered as a constant under fixed solar activity (Fig. 6). On the other hand the rate of [O] association is not limited and any amount of [O] transferred downward will be lost via a three-body collision $O + O + M \rightarrow O_2 + M$, where M is a total number density of neutral species mostly presented by $[N_2]$, the rate of this process exponentially increases with decreasing height. The transfer of [O] is provided by molecular diffusion down to the turbopause level (around 120 km) and further by eddy diffusion, the latter being a fairly fast process. Theoretically it was shown that the maximal value of the time average eddy diffusion coefficient in the thermosphere could not exceed 3×10^6 cm^2/s [55] and this was confirmed experimentally - the annual mean eddy diffusion coefficient is $\sim 4 \times 10^6$ cm^2/s at 85–100 km[56], the same estimate was earlier obtained[15]. This gives the characteristic time for the eddy diffusion transfer of [O] $\tau_{edd} \sim H^2/K_{edd} \sim 1$ day at ~ 100 km. It means that newly produced [O] is very efficiently redistributed over the thermospheric column. Therefore the downward transfer of [O] by eddy diffusion is the process globally controlling the amount of [O] in the whole thermosphere. Anyway it is not seen any other way to explain the global increase of the total amount of [O] during equinoxes as no redistribution of [O] by global circulation can produce additional [O] in the thermosphere.

The results[19,20] apparently confirm this conclusion. The minimal intensity of eddy diffusion in the vicinity of equinoxes qualitatively agrees with the 'thermospheric spoon' mechanism[18] basing on a reasonable idea that under a symmetric heating of the thermosphere during equinoxes global turbulence should be at the minimal level. However TIE-GCM simulations only qualitatively reproduce O/N_2 and neutral density semiannual variations as they are much smaller than observed ones[19]. But the very idea of yearly varying eddy diffusion gives a straightforward explanation to the observed variations of the total [O] abundance (Fig. 6).

According to the mechanism[12] during equinoxes one should expect a strong upwelling from the equatorial latitudes due to strong thermosphere heating. Such upwelling inevitably should be accompanied by a decrease of the [O] abundance. However MSISE00 gives peaks of the total atomic oxygen abundance at the equator during equinoxes under any level of solar activity. Figure 7 gives observed noontime foF_2 monthly medians along with MSISE00 [O] column concentration (above 70 km height) at the equatorial station Boa Vista (2.8^0N, 299.3^0E) under solar minimum in 2019 and maximum in 2014.

Figure 7 gives well-pronounced foF_2 equinoctial peaks of equal magnitude both under solar minimum and maximum which just manifest the corresponding peaks in the total [O] column content. Notice that column [O] reaches its maxima at equinoxes when the upwelling from the equator is supposed to be the largest according to[12] while minimal column [O] content takes place in summer when the subsolar point (and so maximal heating) is far from the equator. This is an obvious contradiction with the mechanism of the atomic oxygen redistribution by global thermospheric circulation[12]. But such variations of atomic oxygen can be explained by seasonal variations of eddy diffusion with minima at equinoxes.

Conclusions

The results of our analysis of semi-annual noontime foF_2 variations at four mid-latitude North Hemisphere stations (Boulder, Rome, Wakkanai, Juliusruh) and two South Hemisphere stations (Hobart, Port Stanley) may be formulated as follows.

Reduced solar activity NmF_2 values manifest a close relationship between autumnal and vernal NmF_2 peaks at the stations in questions. All correlation coefficients are significant at the 99.9% confidence level and vary from 0.680 ± 0.168 at Boulder to 0.896 ± 0.060 at Hobart with the correlation ranging between noticeable and close according to the Ceddok scale.

The NmF_2 autumnal peak on average is larger than the vernal one in both Hemispheres at least under solar minimum. The observed NmF_2 difference in the two peaks is attributed to the difference in thermospheric parameters not related to solar and geomagnetic activity.

Larger $q(O^+)_{max}$ and smaller β_{max} in autumn compared to spring may be considered as the reasons for larger autumnal NmF_2 peak compared to vernal one. The abundance of atomic oxygen plays the leading role in the difference between NmF_2 in the two peaks.

The vernal peak may occur in the course of three months in both Hemispheres while the occurrence of the autumnal peak is confined by two months. This may relate to a fast summer-to-winter transition of the thermosheric circulation which transfers atomic oxygen from summer to winter Hemisphere while the winter-to-summer transition is a more prolonged process under analyzed deep solar minimum conditions. This results in small month-to-month and large day-to-day NmF_2 variations in spring. Under such a scatter the monthly median NmF_2 peak may occur in any of three months in the vicinity of the vernal equinox.

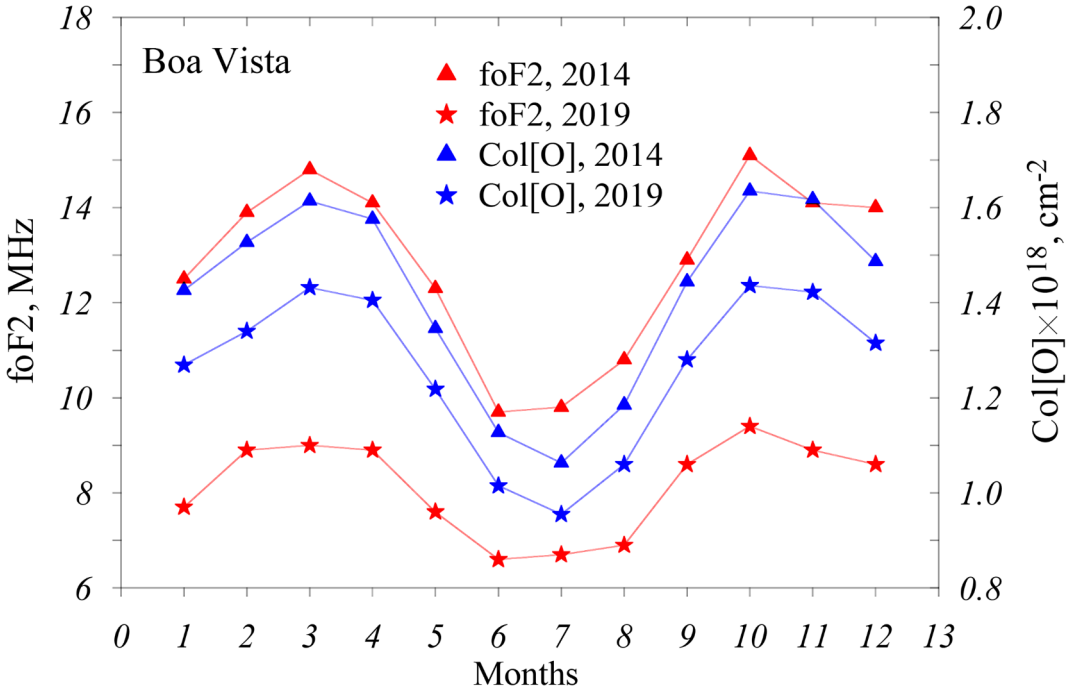

Fig. 7. Yearly variations of noontime foF_2 monthly medians are given along with MSISE00 [O] column concentration under solar minimum (2019) and maximum (2014) at the equatorial station Boa Vista.

A two-hump NmF_2 variation with a trough in December-January (Northern Hemisphere) is a manifestation of low [O] concentration in December-January relative to October/November values rather than the solar zenith angle effect as this was suggested[12]. Solar zenith angle provides some contribution to this NmF_2 decrease but this is not the main factor leading to the midwinter NmF_2 depression.

The global atomic oxygen abundance given by the empirical (based on observations) MSISE00 thermospheric model mainly manifests semiannual variations with close magnitudes in the two peaks both under solar maximum and minimum. This indicates the global increase of the total atomic oxygen abundance during equinoxes. Such an increase cannot be attributed to any redistribution[12,18] of atomic oxygen in the thermosphere as we have the absolute global scale [O] increase.

6. The downward transfer of [O] by eddy diffusion is the process which can globally control the amount of [O] in the thermosphere. Anyway it is not seen any other way to explain the global increase of the total amount of [O] during equinoxes as no redistribution of [O] by global circulation can produce additional [O] in the thermosphere.

Data availability statement

The European Space Agency provides Swarm (https://earth.esa.int/eogateway/catalog/swarm-ionosphere-magnetosphere) the GFZ German Research Center for CHAMP data (ftp://anonymous@isdcftp.gfz-potsdam.de/champ/) and Woods for EUV observations (http://lasp.colorado.edu/lisird/). The Rome ionospheric data are provided by INGV (https://doi.org/10.13127/eswua/hf), as the Lowell DIDBase through GIRO for ionosonde data (http:// giro.uml.edu/). NOAA SWPC (https://www.swpc.noaa.gov/), GFZ Potsdam (https://www.gfz-potsdam.de/en/ kp-index/), the WDC for Geomagnetism, Kyoto (http://wdc.kugi.kyoto-u.ac.jp/wdc/Sect. 3.html) for geomagnetic index ap)

Received: 29 August 2024; Accepted: 21 February 2025
Published online: 25 March 2025

References

1. Yonezawa, T. & Arima, Y. On the seasonal and non-seasonal annual variations and the semi-annual variation in the noon and midnight electron densities of the F2 layer in middle latitudes. *J. Radio Res. Labs.* **6**, 293–309 (1959).
2. Yonezawa, T. The solar-activity and latitudinal characteristics of the seasonal, nonseasonal and semi-annual variations in the peak electron densities of the F2-layer at noon and at midnight in middle and low latitudes. *J. Atmos. Terr. Phys., 33*, 889–907, 1971. (1971).
3. Yonezawa, T. Semi-annual variations in the peak electron densities of the F2- and E- layers. *J. Radio Res. Lab. Jpn.* **19**, 1 (1972).
4. Berkner, L. V., Wells, H. W. & Seaton, S. L. Characteristics of the upper region of the ionosphere. *Terr. Magn. Atmos. Electr.* **41**, 173–184 (1936).
5. Berkner, L. V. & Wells, H. W. Non–seasonal change of F2-region ion density. *Terrest Magn. Atmos. Elec.* **43**, 15–36 (1938).
6. Rishbeth, H. & Müller-Wodarg, I. C. F. Why is there more ionosphere in January than in July? The annual asymmetry in the F2-layer. *Ann. Geophys.* **24**, 3293–3311 (2006).

7. Qian, L., Burns, A. G., Solomon, S. C. & Wang, W. Annual/semiannual variation of the ionosphere. *Geophys. Res. Lett.* **40**, 1928–1933 (2013).
8. Mikhailov, A. V. & Perrone, L. The annual asymmetry in the F2 layer during deep solar minimum (2008–2009): December anomaly. *J. Geophys. Res. Space Phys.* **120**, 1341–1354. https://doi.org/10.1002/2014JA020929 (2015).
9. Rishbeth, H. & Setty, C. S. G. K. The F-layer at sunrise. *J. Atmos. Solar-Terr Phys.* **23**, 263–276 (1961).
10. Wright, J. W. The F-region seasonal anomaly. *J. Geophys. Res.* **68**, 4379 (1963).
11. Mayr, H. G., Harris, I. & Spencer, N. W. Some properties of upper atmosphere dynamics. *Rev. Geophys. Space Phys.* **16**, 539 (1978).
12. Rishbeth, H. et al. Annual and semianual variations in the ionospheric F2-layer: II. Physical discussion. *Ann. Geophys.* **18**, 945–956 (2000).
13. Paetzold, H. K. & Zschőrner, H. An annual and a semiannual variation of the upper air density. *Pure Appl. Geophys.* **48**, 85–92 (1961).
14. Zou, L. et al. Annual and semianual variations in the ionospheric F2-layer: I. *Modelling Ann. Geophys.* **18**, 927–944 (2000).
15. Colegrove, F. D., Hanson, W. B. & Johnson, F. S. Eddy diffusion and oxygen transport in the lower thermosphere. *J. Geophys. Res.* **70**, 4931–4941 (1965).
16. Shimazaki, T. Effective eddy diffusion coefficient and atmospheric composition in the lower thermosphere. *J. Atmos. Terr. Phys.* **33**, 1383–1401 (1971).
17. Schuchardt, K. G. H. & Blum, P. W. Correlation between the homopause height and density variations in the upper atmospheres. *Space Res.* **13**, 335–340 (1977).
18. Fuller-Rowell, T. J. The "thermospheric spoon": A mechanism for the semiannual density variation. *J. Geophys. Res.* **103**, 3951–3956 (1998).
19. Qian, L., Solomon, S. C. & Kane, T. J. Seasonal variation of thermospheric density and composition. *J. Geophys. Res.* **114**, A01312. https://doi.org/10.1029/2008JA013643 (2009).
20. Pilinski, M. D. & Crowley, G. Seasonal variability in global eddy diffusion and the effect on neutral density. *J. Geophys. Res. Space Phys.* **120**, 3097–3117. 10.1002/ 2015JA021084 (2015).
21. Lomidze, L., Knudsen, D. J., Shepherd, M., Huba, J. D. & Maute, A. Equinoctial asymmetry in the upper ionosphere: comparison of satellite observations and models. *J. Geophys. Research: Space Phys.* **128**, e2022JA031123. https://doi.org/10.1029/2022JA03 (2023).
22. Yonezawa, T. On the seasonal and non-seasonal annual variations and the semi-annual variation in the noon and midnight densities of the F2 layer in middle latitudes, II. *J. Radio Res. Lab. Jpn*. **6**, 651 (1959).
23. King, J. W. & Smith, P. A. The seasonal anomaly in the behavior of the F2-layer critical frequency. *J. Atmos. Terr. Phys.* **30**, 1707–1713 (1968).
24. Ivanov-Kholodny, G. S. & Mikhailov, A. V. *The Prediction of Ionospheric Conditions* (D. Reidel Pub. Com., 1986).
25. Woods, T. N., Eparvier, F. G., Harder, J. & Snow, M. Decoupling solar variability and instrument trends using the multiple Same-Irradiance-Level (MuSIL) analysis technique. *Sol Phys.* **293**, 76. https://doi.org/10.1007/s11207-018-1294-5 (2018).
26. Richards, P. C., Fennelly, J. A. & Torr, D. G. EUVAC: a solar EUV flux model for aeronomic calculations. *J. Phys. Res.* **99**, 8981–8992 (1994).
27. Banks, P. M. & Kockarts, G. *Aeronomy* (Academic, 1973).
28. Nusinov, A. A., Kazachevskaya, T. V. & Katyushina, V. V. Solar extreme and Far ultraviolet radiation modeling for aeronomic calculations. *Remote Sens.* **13**, 1454. https://doi.org/10.3390/rs13081454 (2021).
29. Machol, J. et al. An improved Lyman alpha composite. *Earth Space Sci.* **6**, 2263–2272. https://doi.org/10.1029/2019EA000648 (2019).
30. Bilitza, D. et al. The international reference ionosphere 2012—a model of international collaboration. *J. Space Weather Space Clim.* **4** (A07). https://doi.org/10.1051/swsc/2014004 (2014).
31. Shubin, V. N. Global empirical model of critical frequency of the ionospheric *F*2-Layer for quiet geomagnetic conditions. *Geomag. Aeronom*. **57**, 414–425 (2017).
32. Rishbeth, H. & Garriott, O. K. *Introduction To Ionospheric Physics* (Academic, 1969).
33. Perrone, L. & Mikhailov, A. V. A new method to retrieve thermospheric parameters from daytime Bottom-Side Ne(h) observations. *J. Geophys. Research: Space Phys.* **123**, 10,200–10212. https://doi.org/10.1029/2018JA025762 (2018).
34. Mikhailov, A. V. & Perrone, L. Poststorm thermospheric NO overcooling? *J. Geophys. Research: Space Phys.* **125**, e2019JA027122. https://doi.org/ (2020).
10. 1029/2019JA027122.
35. Mikhailov, A., Perrone, L. & Nusinov, A. Mid-Latitude daytime F2-Layer disturbance mechanism under extremely low solar and geomagnetic activity in 2008–2009. *Remote Sens.* **13**, 1514 (2021).
36. Perrone, L., Mikhailov, A. V. & Sabbagh, D. Thermospheric parameters during ionospheric G-Conditions. *Remote Sens.* **13**, 3440. https://doi.org/10.3390/rs13173440 (2021a).
37. Strickland, D. J. et al. Quiet-time seasonal behavior of the thermosphere seen in the Far ultraviolet dayglow. *J. Geophys. Res.* **109**, A01302. https://doi.org/10.1029/2003JA010220 (2004).
38. Mikhailov, A. V. & Perrone, L. Longitudinal variations in thermospheric parameters under summer noontime conditions inferred from ionospheric observations: A comparison with empirical models. *Sci. Rep.* **9**, 12763. https://doi.org/10.1038/s41598-019-49255-1 (2019). https://www.nature.com/articles/s41598-019-49255-1.ris
39. Rishbeth, H. & Barron, D. W. Equilibrium electron distributions in the ionospheric F2-layer. *J. Atmos. Terr. Phys.* **18**, 234–252 (1960).
40. Perrone, L., Scotto, C. & Sabbagh, D. Testing of the method retrieving a consistent set of aeronomic parameters with millstone hill ISR noontime hmF2 observations. *IEEE Geosci. Remote Sens. Lett.* **v.18**, 1545–1700. https://doi.org/10.1109/LGRS.2020.3007362 (2021b).
41. Torr, M. R. & Torr, D. G. The seasonal behaviour of the F2-layer of the ionosphere. *J. Atmos. Terr. Phys.* **35**, 2237–2251 (1973).
42. Perrone, L. & Mikhailov, A. V. Seasonal transitions in the thermosphere inferred from ionospheric observations. *Remote Sens. 2023*. **15** https://doi.org/10.3390/rs15082022 (2022).
43. Olsson, A., Janhunen, P., Karlsson, T., Ivchenko, N. & Blomberg, L. G. Statistics of joule heating in the auroral zone and Polar cap using Astrid-2 satellite Poynting flux. *Ann. Geophys.* **22**, 4133–4142 (2004). SRef-ID: 1432 – 0576/ag/2004-22-4.
44. Fuller-Rowell, T. J., Codrescu, M. V., Moffett, R. J. & Quegan, S. Response of the thermosphere and ionosphere to geomagnetic storm. *J. Geophys. Res.* **99**, 3893–3914 (1994).
45. Prölss, G. W. in *Ionospheric F-region Storms, Handbook of Atmospheric Electrodynamics*. Vol. 2, 195–248 (eds Volland, H.) (CRC Press/Boca Raton, 1995).
46. Forbes, J. M., Gonzalez, R., Marcos, F. A., Revelle, D. & Parish, H. Magnetic storm response of lower thermospheric density. *J. Geophys. Res.* **101**, 2313–2319 (1996).
47. Rishbeth, H. How the thermospheric circulation affects the ionospheric F2-layer. *J. Atmospheric Solar Terr. Phys.* **60**, 1385–1402 (1998).
48. Field, P. R. et al. Modelling composition changes in F-layer storms. *J. Atmos. Solar-Terr Phys.* **60**, 523–543 (1998).
49. Rishbeth, H. & Müller-Wodarg, I. C. F. Vertical circulation and thermospheric composition: a modelling study. *Ann. Geophys.* **17**, 794–805 (1999).
50. Qian, L., Yu, W., Pedatella, N., Yue, J. & Wang, W. Hemispheric asymmetry of the annual and semiannual variation of thermospheric composition. *J. Geophys. Research: Space Phys.* **128**, e2022JA031077. https://doi.org/10.1029/2022JA031077 (2023).

51. Picone, J. M., Hedin, A. E., Drob, D. P. & Aikin, A. C. NRLMSISE-00 empirical model of the atmosphere: statistical comparison and scientific issues. *J. Geophys. Res.* **107**, 1468. https://doi.org/10.1029/2002JA009430 (2002).
52. Emmert, J. T. et al. NRLMSIS 2.0: A whole-atmosphere empirical model of temperature and neutral species densities. *Earth Space Sci.* **7** (3). https://doi.org/10.1029/2020EA001321 (2020). e2020EA001321.
53. Bruinsma, S., Tamagnan, D. & Biancale, R. Atmospheric density derived from CHAMP/STAR accelerometer observations. *Planet. Space Sci.* **52**, 297–312. https://doi.org/10.1016/j.pss.2003.11.004 (2004).
54. Liu, G. et al. Thermospheric temperature and ΣO/N2 variations as observed by GOLD and compared to MSIS and WACCM-X simulations during 2019–2020 at deep solar minimum. *J. Geophys. Research: SpacePhysics*. **128**, e2023JA031560. https://doi.org/10.1029/2023JA0315601123 (2023).
55. Gordiets, B. F., Kulikov, Y. N., Markov, M. N. & Marov, M. Y. Numerical modelling of the thermospheric heat budget. *J. Geophys. Res.* **87**, 4504–4514 (1982).
56. Liu, A. Z. Estimate eddy diffusion coefficients from gravity wave vertical momentum and heat fluxes. *Geophys. Res. Lett.* **36**, L08806. https://doi.org/10.1029/2009GL037495 (2009).

Acknowledgements

This research was carried within: the INGV Pianeta Dinamico Project (CUP D53J19000170001), Space weather Effects on South atlantic Anomaly Region (SESAR)—, funded by MUR (law 145/2018). the Antarctic Thermosphere Retrieved from Ionospheric Observations(ATRIO) funded by Programma Nazionale di Ricerche in Antartide(PNRA18_00282 -A)The authors thanks for the Ionosonde data the GIRO group http://spase.info/SMWG/Observatory/GIROThis publication uses data from: from the Juliusruh Ionosonde which is owned by the Leibniz Institute of Atmospheric Physics Kuehlungsbor; The responsible Operations Manager is Jens Mielich. The authors thanks for the Hobart Ionosonde data the Australian Space Weather Forecasting Center https://www.sws.bom.gov.au/.This Research draws upon data provided by WDC for Ionosphere and Space Weather, Tokyo, National Institute of Information and Communications Technology. https://wdc.nict.go.jp/wdc-top/index.html.

Author contributions

Conceptualization, A.M. ; methodology, A.M. and L.P.; software, A.M.and L.P.; data preparation, L.P. and A.M.; writing, A.M. and L.P. All authors have read and agreedto the published version of the manuscript.

Declarations

Competing interests

The authors declare no competing interests.

Additional information

Correspondence and requests for materials should be addressed to L.P.

Reprints and permissions information is available at www.nature.com/reprints.

Publisher's note Springer Nature remains neutral with regard to jurisdictional claims in published maps and institutional affiliations.